Chapter 1

Radon Detection

The SuperNEMO experiment requires radon contamination of the tracker gas to be less than 0.15 mBq/m^3, and achieving this target has posed a significant challenge in the detector design and construction. Furthermore, the measuring and monitoring of such ultra-low radon activity is also a challenging prospect. The world's best radon detectors can achieve a sensitivity of 0.1 Bq/m^3, which is 3 orders of magnitude away from meeting the SuperNEMO tracker gas radiopurity requirement. As such, a state-of-art custom-made electrostatic detector has been acquired for SuperNEMO. Initially designed for the ELEGANT V and Super-Kamiokande experiments [1, 2], the detector is capable of measuring radon down to a level of 1 - 2 mBq/m^3 — 2 orders of magnitude better than commercial detectors. However, this is still ten times higher than the target sensitivity. A new system called the Radon Concentration Line (RnCL) has been developed and built at UCL, which can concentrate the gas sample so that the sample can reach the sensitivity required for the SuperNEMO detector.

1.1 Electrostatic Detector

The electrostatic detector, as shown in Figure 1.1, consists of the following parts: a 70-litre cylindrical stainless steel detection chamber, a silicon PIN photodiode, electronics associated with the detector, and two valves — inlet and outlet — for

gas flow. To minimise the background, the chamber is electro-polished after welding to reduce the surface area where radioactive particles can be deposited onto. In addition, metallic valves applied with Styrene butadiene rubber (SBR) are used to prevent radon diffusion. The PIN photodiode is electrically isolated from the chamber by a perspex sheet and feedthrough, and is connected to the electronics, which include a high voltage divider and a pre-amplifier housed in the lid of the detector, separated from the chamber. The aim of this design is to provide shielding from external noise as well as to reduce the length of the signal cable before the pre-amplifier. Negative high-voltage, typically -1500 V, is applied to the P-layer of the PIN photodiode while the chamber is grounded, to generate the electrostatic field. Simultaneously, -100 V is separated to provide the inverse bias voltage to the PIN diode through a high voltage divider.

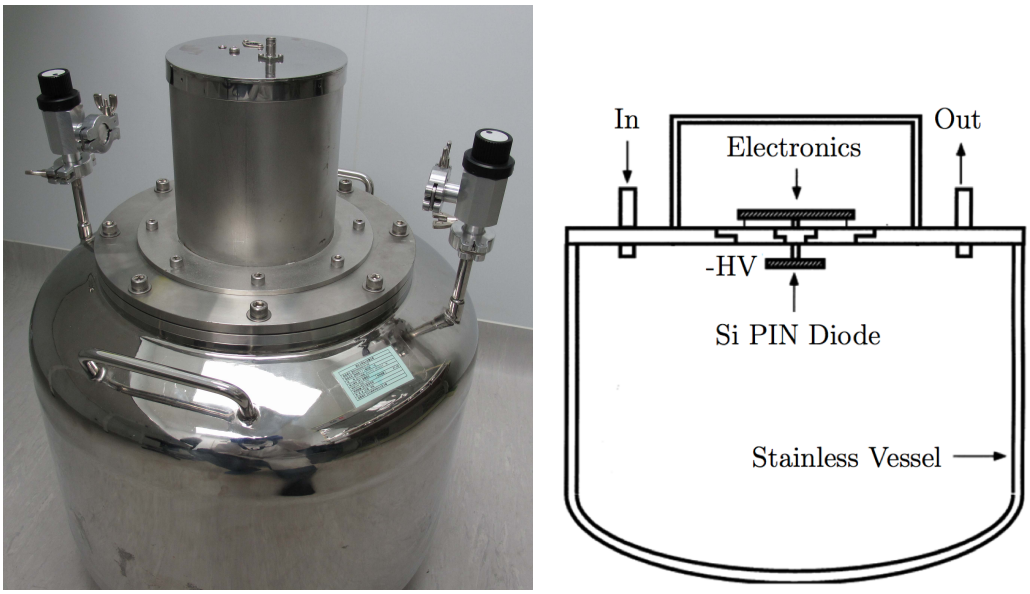

Figure 1.1: (a)The electrostatic detector used for all the radon emanation measurements along with the RnCL and the emanation chamber. (b) The electrostatic radon detector schematic as shown in [1]

The daughter nucleus of ^{222}Rn decay are predominately positively charged. A measurement taken in 1913 shows that 88% of the ions and compounds from radon decay are positively charged [3], which is consistent with the current measurement result, $87.3 \pm 1.6\%$ [4].

Due to the applied electric field, positive ions from radon decay are attracted onto the PIN photodiode. When these ions undergo α decay, they can be detected by the photodiode, and distinguished by the energy deposited on the PIN: 6.1 MeV, 7.9 MeV, and 5.4 MeV for ^{218}Po, ^{214}Po, and ^{210}Po respectively. ^{214}Po has a higher detection efficiency and is generally considered as a measure of radon level. Ideally, one may expect that the collection efficiencies for ^{214}Po and ^{218}Po to be the same; however, not 100% of decay daughters are collected due to neutralisation. The ^{218}Po which has a higher ionisation potential, is more easily to be neutralisied in the environment where only trace amount of impurities are present. ^{210}Pb has a relatively long half-life of 22.3 yrs; hence its daughter nuclei ^{210}Po, will not reach equilibrium with the ^{222}Rn within the time frame of a typical measurement, and it will not characterise the radon concentration.

1.1.1 Detector Signal

The detector signal is passed to the DAQ system: a Nuclear Electronics Miniature box (Wiener NEMbox SU706), which is a field-programmable gate array (FPGA) designed to function as a NIM crate in a small, stand-alone desktop unit. The NEMbox is used to trigger and digitise the pulses for storage, and at the same time, can prevent re-triggering from the afterpulse. The dead time for this system while recording the full signal pulses to disk for offline analysis is $\sim$ 17 ms. A calibrated source of known frequency was used to measure the response of the DAQ system, and the results are as shown in Figure 1.2. In normal data-taking modes, the dead time should contribute a negligible effect, however, for high activity measurement such as a calibration run, it must be taken into account [5].

1.1.2 Detector Efficiency Calibration

The detection efficiency of the electrostatic detector was calibrated to investigate the response of the detector to a known activity of radon. A 1.32 kBq ^{226}Ra flowthrough standard source (Pylon Electronics, RN-1025) was procured for this calibration.

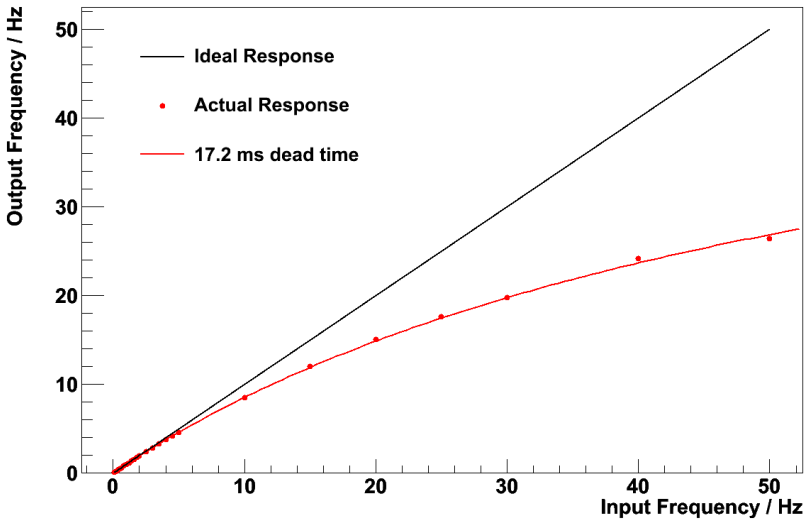

Figure 1.2: Response of the DAQ system for various input frequencies, where the red dots show the measured response, and the red line shows the expected response when the dead time between two pulses is 17.2 ms [5].

The design of the source allows the gas to flow through the source material, which can ensure that all the emanated radon is exhausted and offer considerable flexibility in the amount of radon for different measurement uses. There are generally two separate methods to calibrate the detector. The first, dubbed the spike method, is to purge a known amount of radon into the detector and measure the activity with the detector. The second, the flowthrough method, is to measure the radon level inside the detector while continuously flushing the radon-carrying gas through the detector over 24 hours. Though both helium or nitrogen can be used as the carrier gas, helium is the preferred choice in this case as impurities in the nitrogen such as nitrous oxides may result in neutralisation of positive ions of radon progenies. The detection efficiency was determined by taking the ratio of the measured activity of radon in the detector chamber over the calculated radon activity introduced from the flowthrough source. In the latest spike method calibration measurement (the spectrum for which is shown in Figure 1.3), for ^{214}Po, the detector can reach a relatively high detection efficiency of $33.3 \pm 1.6\%$ and for ^{218}Po the efficiency is $29.1 \pm 1.4\%$(see Figure 1.4).

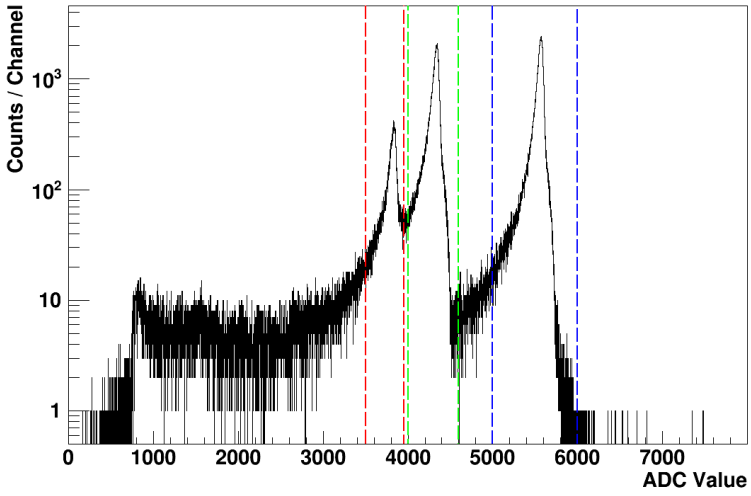

Figure 1.3: The energy spectrum with peaks of ^{210}Po, ^{218}Po, and ^{214}Po from left to right during the detector detection efficiency calibration run.

Comparing with the previous two efficiency calibrations summarised in Table 1.1, one can conclude that the detector performed stably over the years even after the HV module upgrades in 2015.

Year of calibration	Efficiency for ^{214}Po	Efficiency for ^{218}Po
2012	$31.6 \pm 1.6\%$	$27.1 \pm 1.4\%$
2014	$31.5 \pm 1.3\%$	$28.14 \pm 1.1\%$

Table 1.1: The results of the last three spike method detection efficiency calibrations.

Practically, the ^{218}Po efficiency can also be affected by peak proximity from the residential ^{210}Po, which is a decay product of ^{210}Pb in the ^{222}Rn decay chain. ^{210}Pb has a relatively long half-life of 22.2 years, which means it will deposit and accumulate on the PIN photodiode during the measurement. In normal low-activity measurements, the ^{210}Po peak is much larger than the ^{218}Po peak, as shown in Figure 1.5. Although the detector resolution is excellent, an overlap between the ^{210}Po and ^{218}Po tail is inevitable. Thus ^{214}Po is the ideal candidate as the measure of radon.

The assumption of the neutralisation effect caused by the extra impurities in the nitrogen environment, mainly trace nitrogen oxides, was confirmed by comparing the calibration results using helium and nitrogen. Lower efficiencies were indeed

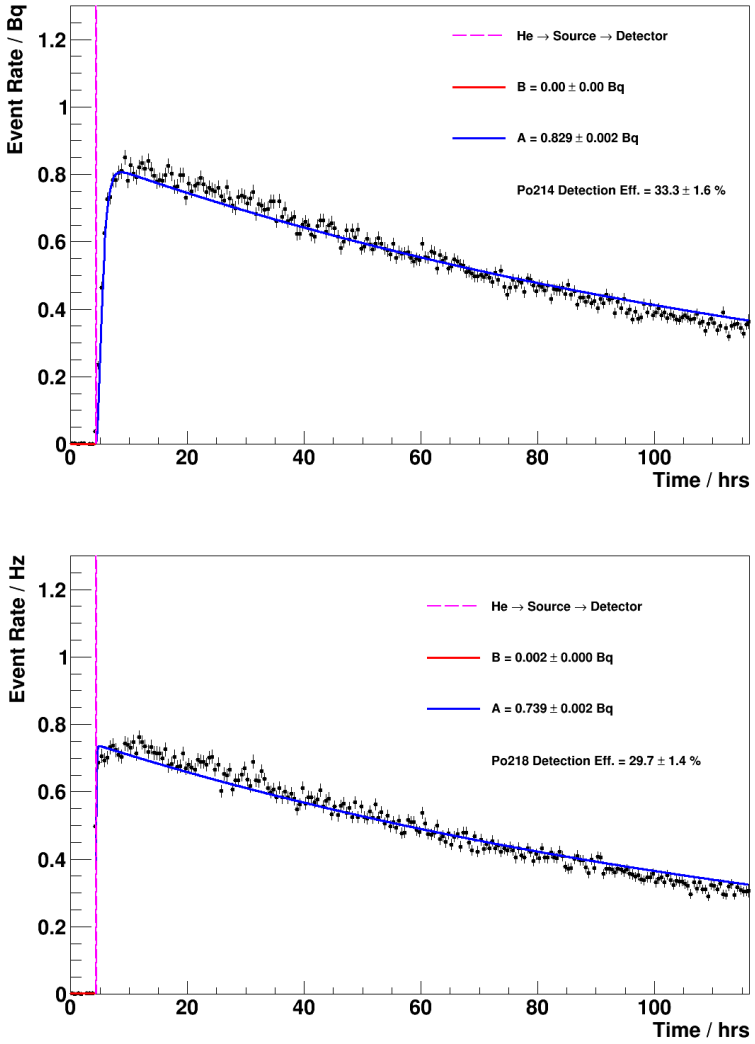

Figure 1.4: Event rates of ^{214}Po on the top and ^{218}Po on the bottom during the spike method detector detection efficiency calibration run, where blue lines show fit with the fixed half-life of ^{222}Rn.

observed: $28.1 \pm 1.1\%$ and $22.3 \pm 0.8\%$ for ^{214}Po and ^{218}Po respectively[6].

The flowthrough method was generally used as a cross-check with the spike calibration. Nitrogen was chosen as the carrier gas flushing through the source and the detector at 4.2 lpm. Taking the ratio of the observed radon level by the detector over the calculated equilibrium radon activity supplied by the source at this flowrate, the detection efficiency can be determined as $26.3 \pm 1.8\%$ and $22.2 \pm 1.6\%$ for ^{214}Po and ^{218}Po respectively. These agree well with the spike method results.

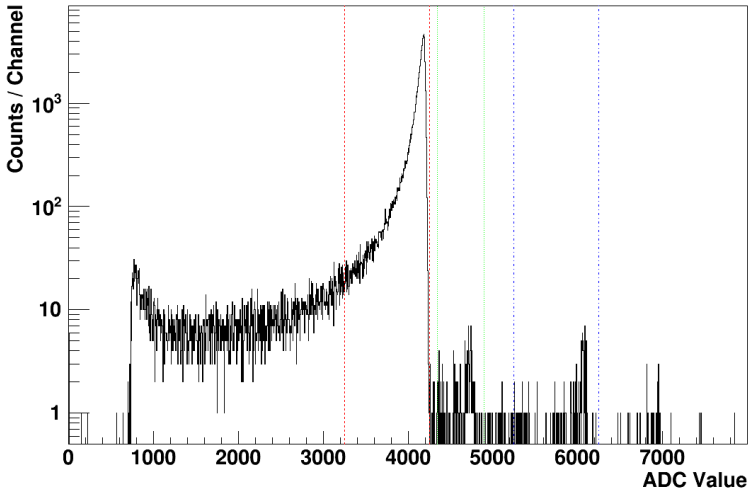

Figure 1.5: The energy spectrum with peaks of ^{210}Po, ^{218}Po, and ^{214}Po from left to right during a typical low-activity measurement.

A summary of the most recent calibration results is shown in Table 1.2.

Calibration Method	Carrier Gas	Efficiency for ^{214}Po	Efficiency for ^{218}Po
Spike	Helium	$33.3 \pm 1.6\%$	$29.1 \pm 1.4\%$
Spike	Nitrogen	$28.1 \pm 1.1\%$	$22.3 \pm 0.9\%$
flowthrough	Nitrogen	$26.3 \pm 1.8\%$	$22.2 \pm 1.6\%$ ~~height~~

Table 1.2: Electrostatic radon detector detection efficiency calibration results using different carrier gas.

1.1.3 Detector Background and Anti-Radon Bag

A sensitive detector requires not only a high detection efficiency but also a low background counting rate. Prior to the measurement of the sample, to accurately estimate the background from the activity of observed radon and to make sure the background is low and stable, a background measurement was carried out. Long-term background measurements were performed occasionally to ascertain the intrinsic activity of the detector. During these kinds of measurements, the detector works in a pure helium environment to maximise the detection efficiency. In a typical detector background measurement (as shown in Figure 1.6), the counting rate of ^{214}Po was found to be 6.5 ± 1.0 counts per day (cpd), translating into 0.23 ± 0.03 mBq or 3.23 ± 0.49 mBq/m^3 given that the detector chamber is 70L in volume.

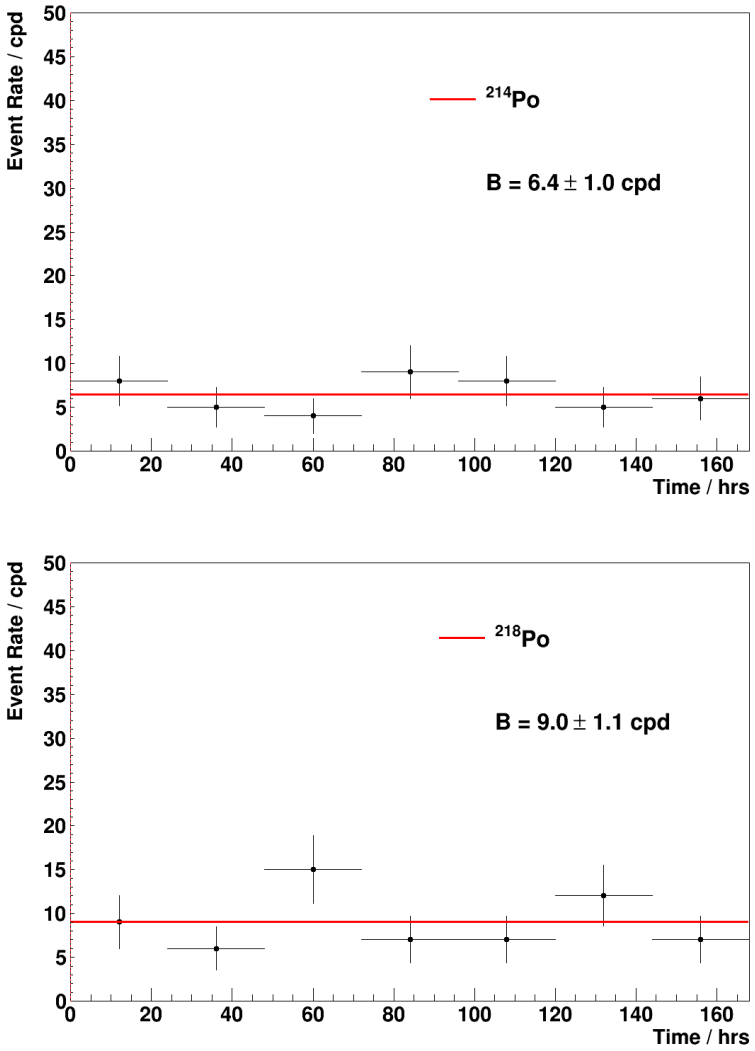

Figure 1.6: Event rates of ^{214}Po on the top and ^{218}Po on the bottom during a typical detector background run.

In a detector calibration run, high activity from the introduced source results in spectral peaks arising from ^{214}Po and ^{218}Po decay. In a background measurement run, the spectra resemble those of low-activity sample measurements.

^{210}Po activity remains close to constant on account of the long half-life of its grand-parent ^{210}Pb deposited on the PIN photodiode, except after a calibration run when its activity will increase. This property of ^{210}Po provides a very convenient way to check the stability of the detector, the power supply, and the DAQ. The detector and the whole system along with it were transported back to a clean room at UCL

from the Mullard Space Science Laboratory (MSSL) in October 2017. After re-assembling, the results from the commissioning run showed that the detector was stable, and the background was low, as expected. A series of long background measurements were taken to verify the background level of the detector, and over a long period, the observed ^{214}Po counting rate remains 5-6 cpd, which is low and stable compared to the background level before the move. However, substantially higher background rates of $\sim$15 cpd were observed later, which will reduce the sensitivity by a factor of $\sqrt{3}$.

One assumption for this increase was the higher radon diffusion effect caused by the abnormal environmental radon level in the cleanroom. The SBR used to coat the seal between the chamber and the lid of the detector as a radon barrier could have aged over seven years. A commercial electrostatic radon detector, RAD7, was then installed to monitor the environmental radon level. Some consistency between the detector background and the environmental radon level was found by comparing the detector data and the RAD7 data during the same period. In addition, the radon level in the room was too high for a clean room (see Figure 1.7).

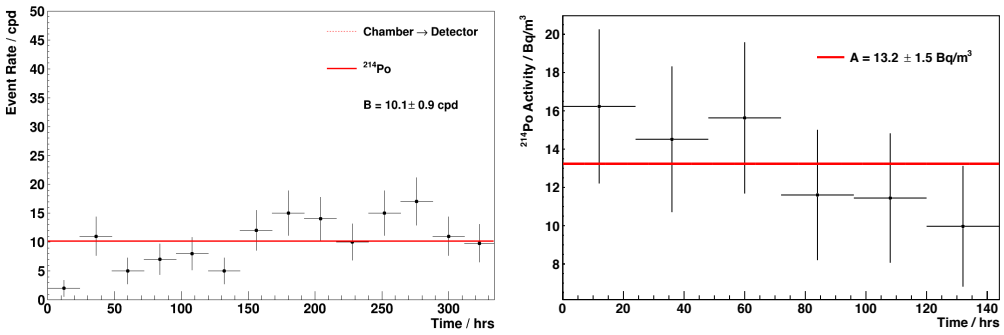

Figure 1.7: Electrostatic detector background (left). The environmental radon level measured by RAD7 during the last six days (right).

Two strategies exist for the attempted mitigation of the high background. The first strategy is to re-coating the seals with SBR, which will inevitably require the opening and re-sealing of the detector, during which process fragile electronic components run the risk of being damaged. In addition, despite being opened in a cleanroom, proper cleaning of the detector chamber post-unsealing to ensure it is

sufficiently uncontaminated is a non-trivial process.

The second solution was chosen as it is both reliable and more convenient than the first one, which is to provide the detector with a clean working environment by housing it in a compatibly sized anti-radon bag where nitrogen is continuously flushed through to suppress radon (as shown in Figure 1.8).

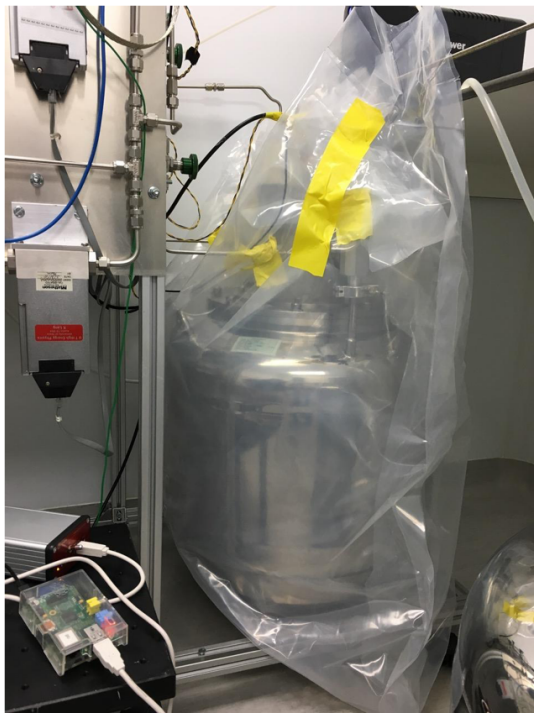

Figure 1.8: Radon detector housed in the anti-radon bag

Double-layer transparent polythene foil was heat-sealed to build the anti-radon bag housing the detector, and two gas feedthroughs were attached to the bag for the gas inlet and outlet. Flushing at 1 lpm, which is the lowest flowrate the ball-flowmetre can achieve, the improvement on the intrinsic background level was observed, with the ^{214}Po rate dropping down to 2.5 - 3.0 mBq/m^3 as usual.

1.1.4 Analysis Method

For offline analysis, each signal is stored via the NEMbox DAQ system as an event in which the date and time together with 1000 sample points of the digitised pulse are recorded in text format. 1000 events fill up a text file, and then the files are

analysed using ROOT.

The data file is processed in two steps. Firstly, a peak-finding algorithm determines the number of peaks in each pulse, their amplitude, and the time — this process is called signal identification. With amplitude and time information, all the pulses can be classified into four different types of events: signal events, BiPo events, pile-up events, and noise events (as shown in Figure 1.9).

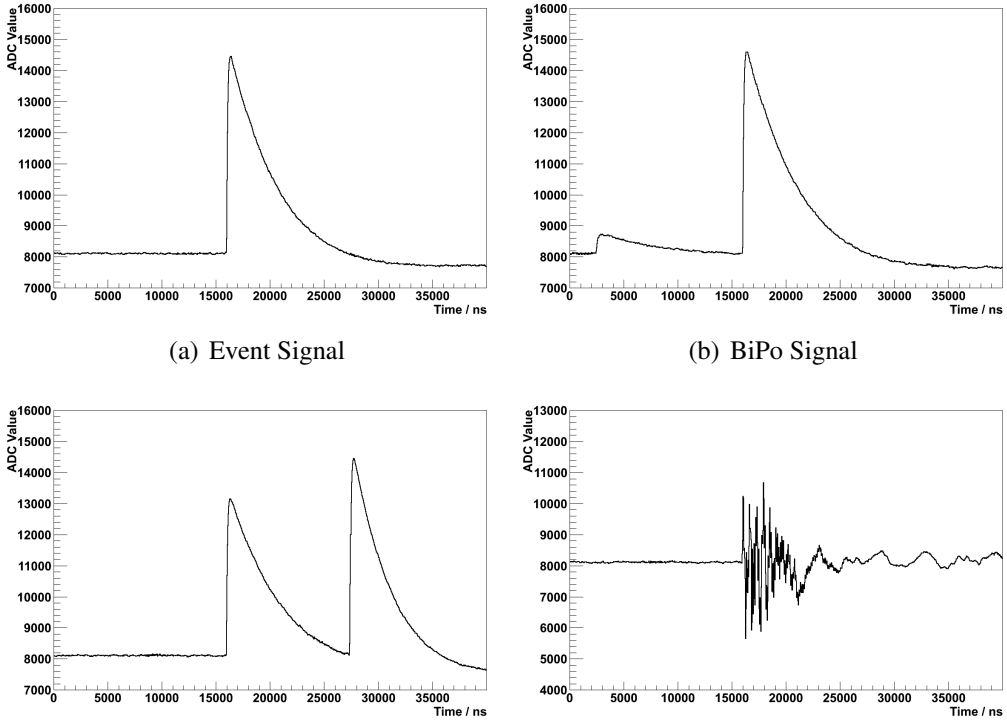

(a) Event Signal (b) BiPo Signal

(c) Pile-up Signal (d) Noise Event

Figure 1.9: Examples of the four types of events identified at the filtering stage.

A signal event contains only one peak, and therefore processing proceeds straight to the next step. The BiPo event refers to the double peak as a result of the electron from ^{214}Bi decay and the alpha from ^{214}Po decay, with an average gap of 164.3 μs, which is the half-life of ^{214}Po. To be detected and identified as a BiPo event, the two particles must deposit energy on the PIN photodiode within the 15 μs pre-trigger window. Thus, this kind of event is rarely observed and contribute only $\sim$1% of the ^{214}Po events. The pile-up event is also a rare, double-peak event, which is distinguishable from the BiPo event as the magnitude of the electron peak is visibly

smaller than the alpha peak due to the decay energy. Pile-up events are typically only observed during calibrations when the activity inside the detector chamber is high. The last type of event is the electronic noise which consists of many peaks of similar magnitude in a single pulse. Their amplitude usually is low; however, very occasionally, one can be large enough to mimic a signal event.

Signal events are then processed to the next, pulse-fitting step. For optimisation of extracting the best value of amplitude, each signal pulse is fitted with a function defined as the ideal form of a signal coming from the PIN photodiode and processed through the pre-amplifier. This signal form can be determined via the observation of the output from the pre-amplifier while injecting light from an LED into the photodiode. The study shows that the signal pulse can be described as a sharp linear rise followed by an exponential decay (see Figure 1.10 as an example).

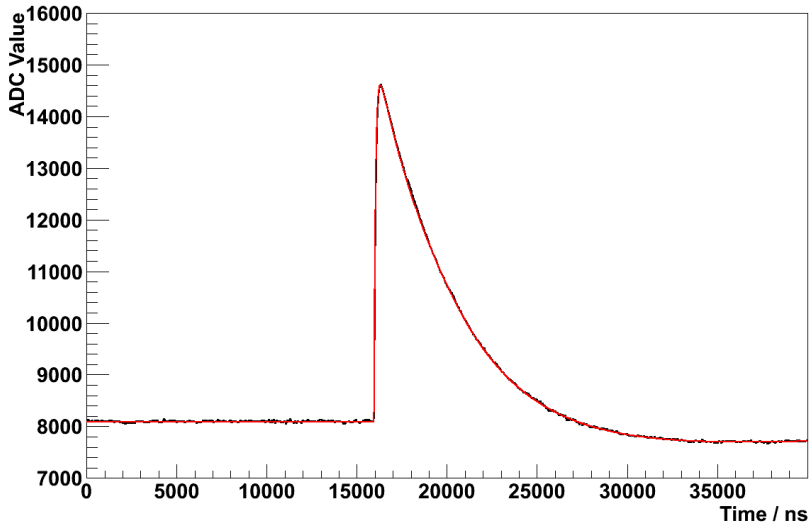

Figure 1.10: A typical signal event (black) with the pulse fitting function (red) superimposed [5].

.

1.2 Sensitivity of the Radon detector

The sensitivity of the radon detector system is quantified by the Minimum Detectable Activity (MDA),as defined in 'Radiation Detection and Measurement' by G.

F. Knoll [7]. In this thesis, the MDA represents the detector sensitivity at 90% unless specifically stated. This definition is based on the binary decision of whether the output of the detector is signal with background or background only. There is the possibility of a false-positive event where a background event is indicated as a signal, in addition to the possibility of a false-negative event where a signal is misidentified as a background only. A critical number of counts, n_c, is predefined, where if more counts than this number are observed, one can claim that the signal presents. n_c is found for the expected number of background events, B, and the measurement confidence level, CL. The probability of false positive is less than $1-\mathrm{CL}$. If B follows the Poisson distribution, to meet the above criterion, n_c is increased until the following inequality is satisfied:

$$P_B(n \geq n_c) = \sum_{n=n_c}^{\infty} Pois(n;B) = 1 - \sum_{n=0}^{n_c-1} e^{-B}\frac{B^n}{n!} \leq 1-\mathrm{CL} \tag{1.1}$$

When n_c has been set high enough to reduce the false-positive probability to $1-\mathrm{CL}$, the probability for false negatives can be used to calculate the minimum expected number of signal events, S, that satisfies the MDA requirement. Thus, S must be increased to satisfy the following inequality:

$$P_{S+B}(n < n_c) = \sum_{n=0}^{n_c-1} Pois(n;S+B) = \sum_{n=0}^{n_c-1} e^{-(S+B)}\frac{(S+B)^n}{n!} \leq 1-\mathrm{CL} \tag{1.2}$$

In Figure 1.11, the black curve is the Poisson-distributed background expectation, from which n_c has been set so that the black-shaded area corresponding to the false-positive equals $1-\mathrm{CL}$. The red line represents the distribution for the minimum signal on the same background, where S has been set such that the red-shaded area also corresponding to the false-negative equal to $1-\mathrm{CL}$. The minimum signal can be converted into an activity which is referred to as the MDA.

.

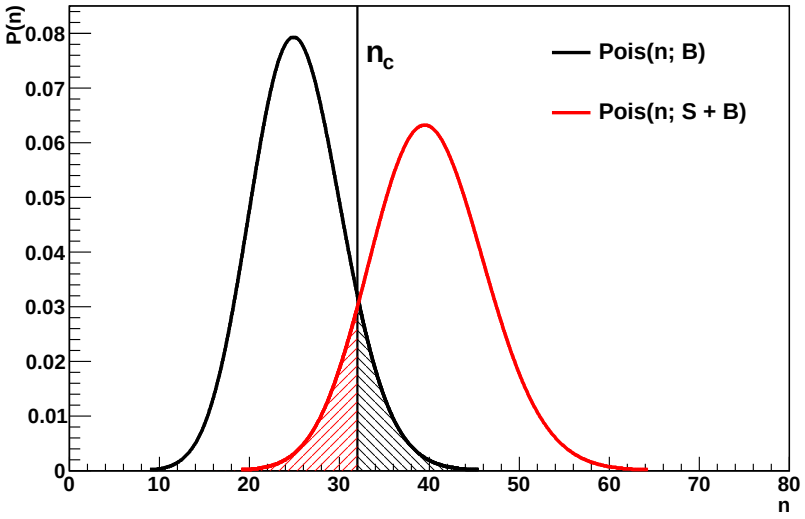

Figure 1.11: Probability distributions for two Poisson distributed variables. n_c has been increased until the false-positive result corresponding to the black-shaded area has sufficiently low probability. S has then been increased until the red-shaded area corresponding to the false-negative result also has area $1-\mathrm{CL}$.

1.2.1 Normal Approximation

As it is difficult to work with the Poisson distributions analytically, simplification is applied based on the normal approximation for a sufficiently large sample size, λ.

$$Pois(\lambda) \approx Norm(\mu = \lambda, \sigma = \sqrt{\lambda}) \tag{1.3}$$

The continuity correction $n_c \to n_c - \frac{1}{2}$ can be used to further improve the approximation. Therefore Equation 1.1, where $\lambda = B$, becomes:

$$P_B(n \geq n_c) \approx \int_{n_c-\frac{1}{2}}^{\infty} \frac{1}{\sqrt{2\pi B}} e^{-\frac{(x-B)^2}{2B}} dx = \frac{1}{2} - \frac{1}{\sqrt{\pi}} \int_0^{\frac{n_c-\frac{1}{2}-B}{\sqrt{2B}}} e^{-t^2} dt \tag{1.4}$$

Introduce the error function defined as:

$$\mathrm{erf}(x) = \frac{2}{\sqrt{\pi}} \int_0^x e^{-t^2} dt \tag{1.5}$$

Using this definition and Equation 1.1 and 1.4 it can be seen that:

$$P_B(n \geq n_c) \approx \frac{1}{2}\left(1 - \mathrm{erf}\left(\frac{n_c - \frac{1}{2} - B}{\sqrt{2B}}\right)\right) \leq 1 - \mathrm{CL} \tag{1.6}$$

The equivalent procedure can be applied to Equation 1.2 to give:

$$P(n < n_c) \approx \frac{1}{2}\left(1 + \mathrm{erf}\left(\frac{n_c - \frac{1}{2} - (S+B)}{\sqrt{2(S+B)}}\right)\right) \leq 1 - \mathrm{CL} \tag{1.7}$$

As the MDA definition provides the smallest possible value of S for a given B, n_c can be eliminated. Combining Equation 1.6 and 1.7, it can be found that:

$$S - \sqrt{2B}E \geq \sqrt{2(S+B)}E \tag{1.8}$$

where E is a positive number defined as:

$$E = \mathrm{erf}^{-1}(2\mathrm{CL} - 1) \tag{1.9}$$

The unphysical solution where $S \leq 0$ should be excluded, so that:

$$S \geq 2E(E + \sqrt{2B}) \tag{1.10}$$

When the inequality is equal, S can reach its minimum value. The MDA can be calculated from the minimum number of signal events that are detectable, S_0, given by:

$$S_0 = 2E(E + \sqrt{2B}) \tag{1.11}$$

1.2.2 Detector Sensitivity

To estimate the detector sensitivity, we assume that a sample with activity A_S introduced into a detector of which intrinsic background activity is A_D. The number of

radon atoms in the detector, N, is given as:

$$\frac{dN}{dt} = -\lambda N + A_D \tag{1.12}$$

Therefore:

$$\frac{d}{dt}(e^{\lambda t}N) = e^{\lambda t}(\frac{dN}{dt} + \lambda N) = e^{\lambda t}A_D \tag{1.13}$$

and:

$$e^{\lambda t}N = \int e^{\lambda t}A_D dt = \frac{A_D}{\lambda}e^{\lambda t} + C \tag{1.14}$$

The detector is flushed to remove residual radon before a measurement, so $N = A_S/\lambda$ at t=0. Thus, C can be determined as $C = A_S/\lambda - A_D/\lambda$, and the number of the radon atom can be calculated as:

$$N = \frac{A_D}{\lambda}(1 - \lambda e^{\lambda t}) + \frac{A_S}{\lambda}e^{-\lambda t} \tag{1.15}$$

Equation 1.15 contains two terms: the background and the signal. When the measurement time is much longer than the half-lives of intermediate isotopes in the decay chain of 222 to 214, one can make the approximation that the signal events are all from 222 since 214 can reach equilibrium after 4.5 hours.

For a zero background detector with the detection efficiency, ε, when sample activity is A_S introduced, the number of signal events after a time T, is given as:

$$S = \varepsilon \int_0^T \lambda N dt = \varepsilon \int_0^T A_S e^{-\lambda t} dt = \varepsilon \frac{A_S}{\lambda}(1 - e^{-\lambda t}) \tag{1.16}$$

Similarly, if the detector has intrinsic background of A_D, when no sample is introduced, the pure background is measured as:

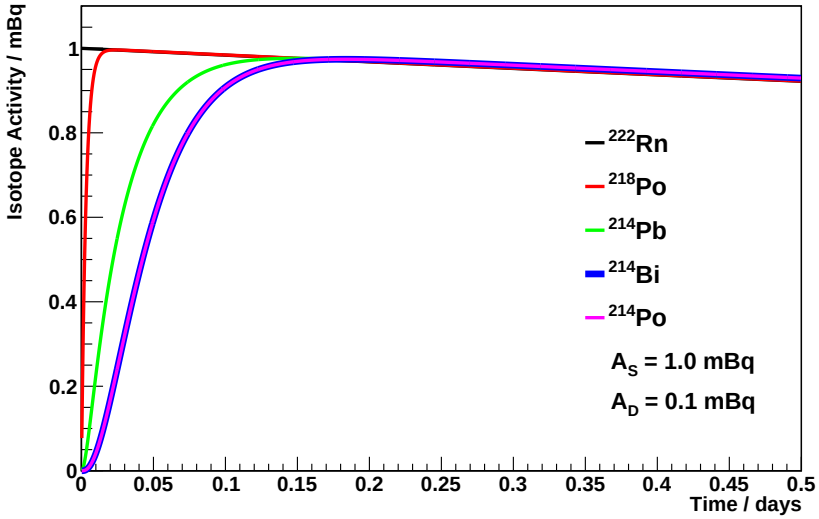

Figure 1.12: Activities of different isotopes in the 222 decay chain with respect to time after introducing 1 mBq of 222 into a detector with 0.1 mBq background [5].

$$B = \varepsilon \int_0^T \lambda N dt = \varepsilon \int_0^T A_D(1-e^{-\lambda t})dt = \varepsilon A_D T - \varepsilon \frac{A_D}{\lambda}(1-e^{-\lambda t}) \qquad (1.17)$$

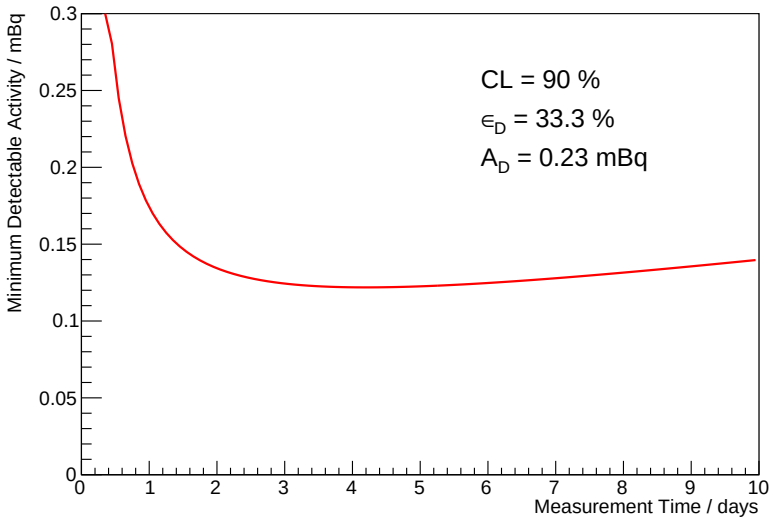

Figure 1.13: MDA for the electrostatic detector as a function of the measurement time.

1.3 Emanation Chambers

In the radon emanation measurements for small samples, the emanation chambers were used to house the sample while isolating it from the environment. Two emanation chambers were built in the US with stainless steel to ensure radiopurity, and then assembled and tested for the intrinsic radon emanation level at UCL.

The emanation chambers (as seen in Figure 1.14) are both 152.4 mm in length and 146 mm in diameter, and each a resulting $\sim$2.6 litres in volume. Two flanges are sealed to the tubular body on both sides, using copper gaskets. The chamber was cleaned, assembled, and leak tested at UCL. A typical leak test contains two stages. In the first stage, helium was used for flushing the chamber to remove residual air once the chamber was assembled, and during flushing, a helium sniffer (GasCheck Tesla Helium Leak Detector, Ion Science) was used to check all the connections to ensure that there were no significant leaks above 10^{-6} cc/s. The leak checking was then repeated after the chamber was sealed under 0.5 bar overpressure, to ensure there were no leaks above 10^{-6} cc/s. The chamber was transported to MSSL for further cleaning, reassembling, and connecting to the gas line, together with the radon detector for further tests (as shown in the schematic Figure 1.15). Leak tests are also carried out each time when it is opened and re-sealed for a sample insertion.

.

.

1.3.1 Background of the Emanation Chambers

The intrinsic background of the chamber determines the sensitivity, and as such it is very important to monitor it by performing the chamber self radon emanation measurement. To prepare for this measurement, the chamber was flushed with 100 volume of helium to remove residual gases, while the helium sniffer was used to carry out a leak test again to ensure for airtightness. After flushing, the chamber was then sealed under atmospheric pressure and left to emanate over 30 days, equi-

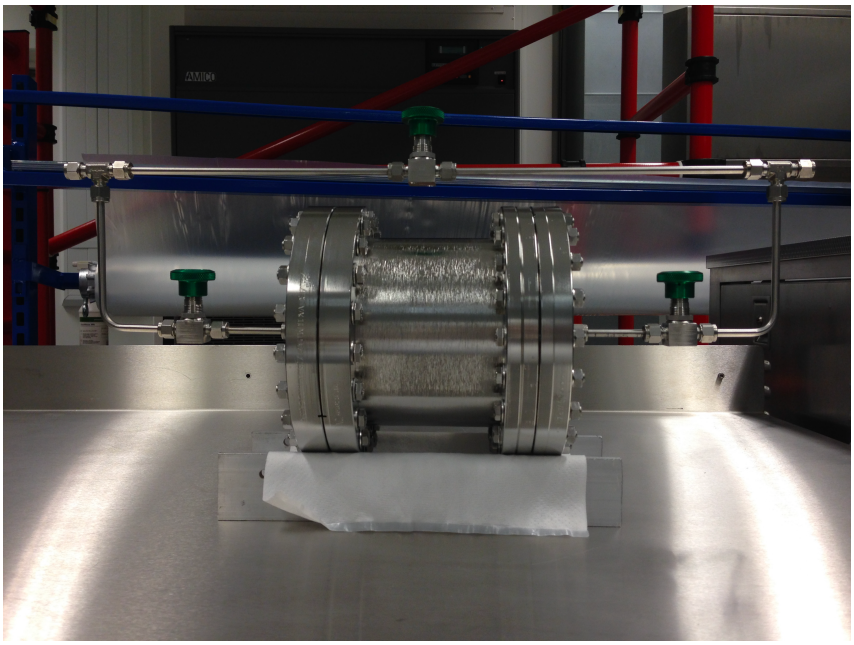

Figure 1.14: Two emanation chambers fully assembled at MSSL.

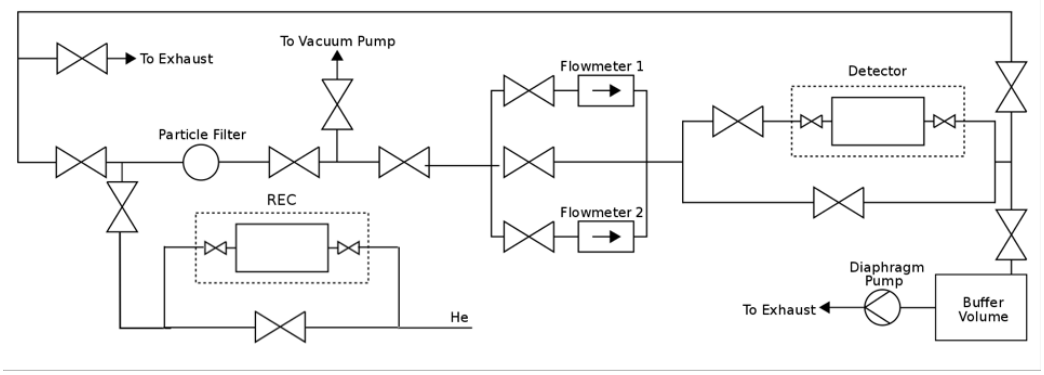

Figure 1.15: The emanation chamber connected to the gas line, along with radon detector.

valent to 8 radon half-lives, to reach equilibrium before being transferred into the detector. Meanwhile, prior to the transfer, the detector was cleaned by flushing 10 volume of clean helium and sealed under atmospheric pressure, followed by a 5-day detector background measurement to not only to ensure the background was low and stable but also to provide an accurate background level during the period. The gas sample was then transferred into the detector for measurement, carried by 25 litres of helium, resulting in an increase of the operational pressure of the detector from 1 bar to 1.36 bar. The first emanation chamber which was assembled in 2014 has an intrinsic background of $<90\mu$Bq at 90% CL [8]. The measurement result of the

second chamber over 8 days is shown in Figure 1.16. Data of the detected signal events each day is plotted with an error bar. The red vertical dashed line indicating the time of sample transfer divides the plots into two parts. The data on the left, referring to the detector background measurement, is fitted with a polynomial to extract the detector background B. For the right side, corresponding to the chamber measurement, an exponential fit based on the radon decay with a half-life of 3.8235 days was applied. The radon activity, A, can be determined by extrapolating back to the moment of transfer. The intrinsic background of the chamber can be calculated

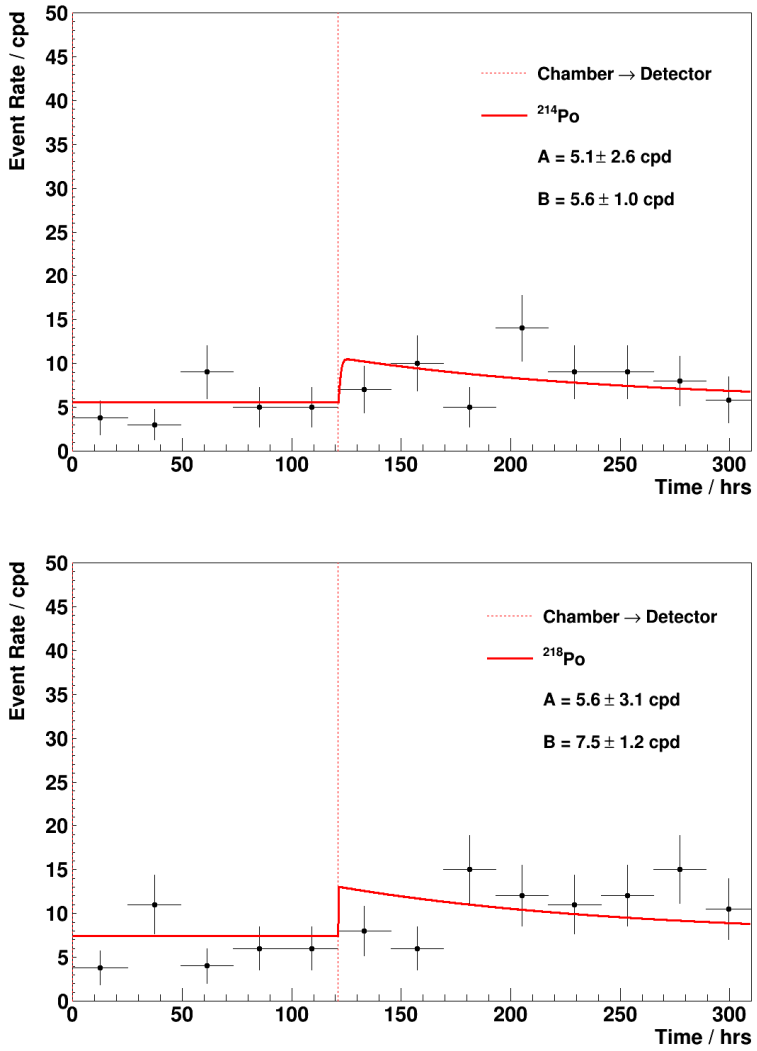

Figure 1.16: Event rates of ^{214}Po and ^{218}Po of the background measurement of the second chamber.

by:

$$A_C = \frac{A\,(cpd) \times 1000\,(mBq)}{\varepsilon_D \times (1 - e^{-N_v}) \times (1 - e^{-\lambda t}) \times 86400\,(secs/day)} \tag{1.18}$$

where A_C is the radon activity in mBq, ε_D is the detection efficiency of the detector, $1 - e^{-\lambda t}$ is the correction of initial activity levels from equilibrium, and N_v is the number of volumes of the chamber flushed into the detector, thus $1 - e^{-N_v}$ gives correction on transfer efficiency.

Hence, the sensitivity (90% C.L.) of the second emanation chamber is:

$$\begin{aligned} A_{^{214}Po} &< 170\mu\text{Bq} \\ A_{^{218}Po} &< 223\mu\text{Bq} \end{aligned} \tag{1.19}$$

1.3.2 Radon Harbouring Hypothesis

For most sample radon emanation measurements, at least a second measurement is carried out to confirm the result. In some of the cases, higher activities than expected were observed in the first radon emanation measurement from some materials compared to further repeat measurements. One possible explanation is the radon harbouring hypothesis. Environmental radon can diffuse into the materials, and this residual radon can not be removed by flushing, and will eventually contribute to the final result.

One good demonstration of this hypothesis is the radon emanation measurement of RTV, which was one of the proposed materials for the SuperNEMO detector. The sample was cleaned and placed into an emanation chamber. The chamber was then flushed with 200 volumes of clean helium to remove residual radon and sealed.

After 30 days emanation, the gas sample was transferred into the detector for the first measurement by purging with 25 litres of clean radon-free helium. After the transfer, the chamber was kept closed, flushed again, and sealed to prepare for a second measurement. After a further 16-day emanation (total time in chamber

days), the gas sample was transferred into the detector. The result found was that the first measurement was surprisingly much higher than the second one. As such, a third transfer was carried out. This time, the material was kept inside the chamber over 80 days, and the emanation since flushing after the second transfer was 20 days. The results from the three measurements are shown in Figure 1.17.

1.4 Radon Concentration Line

The sensitivity of the electrostatic radon detector at UCL is one of the best in the world. However, it is still not enough to measure the SuperNEMO target radon background level 150 μBq/m^3. The detector is 70 litres in volume and can not be operated with too much overpressure, and is thus almost impossible to improve the sensitivity of by increasing the gas sample volume purged into the detector. However, there is still another possibility which is to increase the radon concentration level so that the total amount of radon can be detectable for the electrostatic detector.

A Radon Concentration Line (RnCL) has been developed and built at UCL, which can concentrate and store radon from large volumes of gas and then sends the sample to the electrostatic detector for measurement.

The RnCL working in conjunction with the electrostatic radon detector can reach a sensitivity of μBq/m^3 [5]. The design of RnCL is based on previous work of MoREx at Heidelberg [9], but has been modified to be more portable. The real-life set-up of RnCL is shown in Figure 1.18.

1.4.1 Setup of the RnCL

The essential part of RnCL is a stainless steel trap containing 52.5 g of radio-pure activated carbon (from Carbo-Act international). In order to improve radon absorption efficiency of the activated carbon, an immersion cooler (the EK90 Immersion Cooler from Thermo Scientific, capable of cooling to a minimum temperature of -90 °C) was used to cool the carbon trap to -50 °C [6].

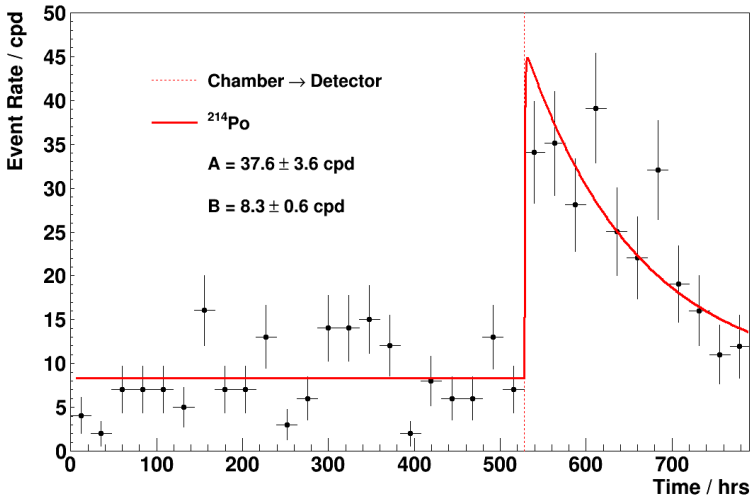

(a) Black Mumba Measurement 1

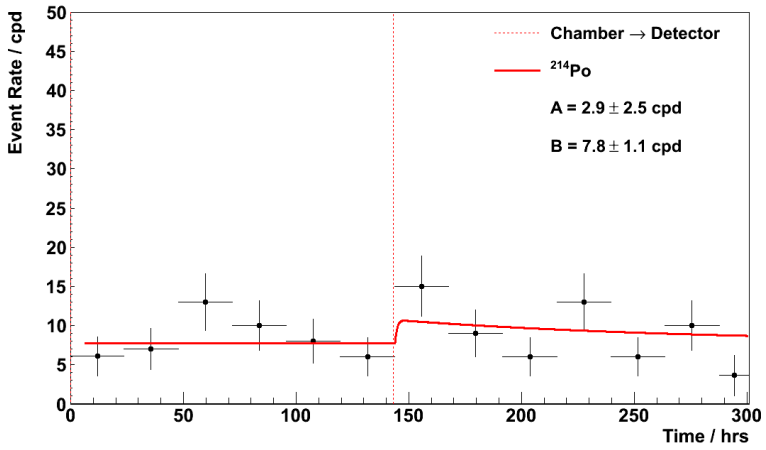

(b) Black Mumba Measurement 2

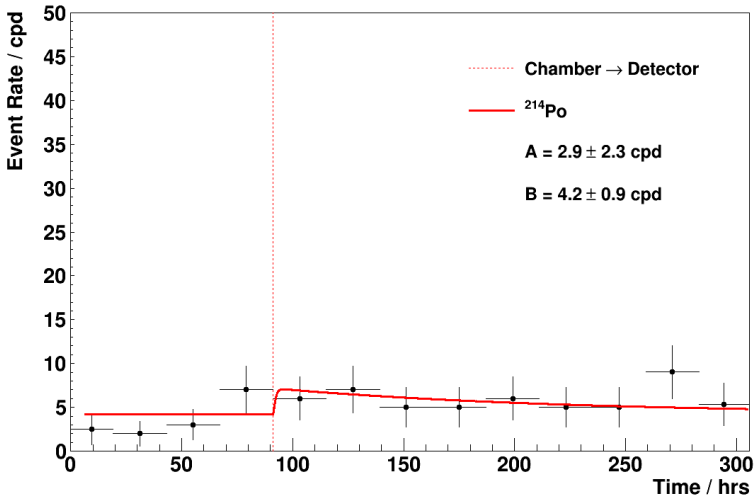

(c) Black Mumba Measurement 3

Figure 1.17: Event rates of ^{214}Po during the first, second, and third measurement of RTV sample shown in (a), (b), and (c) respectively.

While flushing gas through the system, radon will be captured in the trap, and this is called the trapping stage. After the trapping stage, the trap will be sealed and warmed to room temperature, then heated to over 220 °C to release radon in preparation for transfer of the radon sample into the detector. The volume of the trap is 0.5 litres in volume, thus in a typical run, 25 litres of flushing gas is assumed to be enough to transfer all the released radon into the detector.

To avoid any particles entering the electrostatic detector, a series of Swagelok stainless steel filters are installed before and after the trap on the gas line. The setup of RnCL is shown in Figure 1.18.

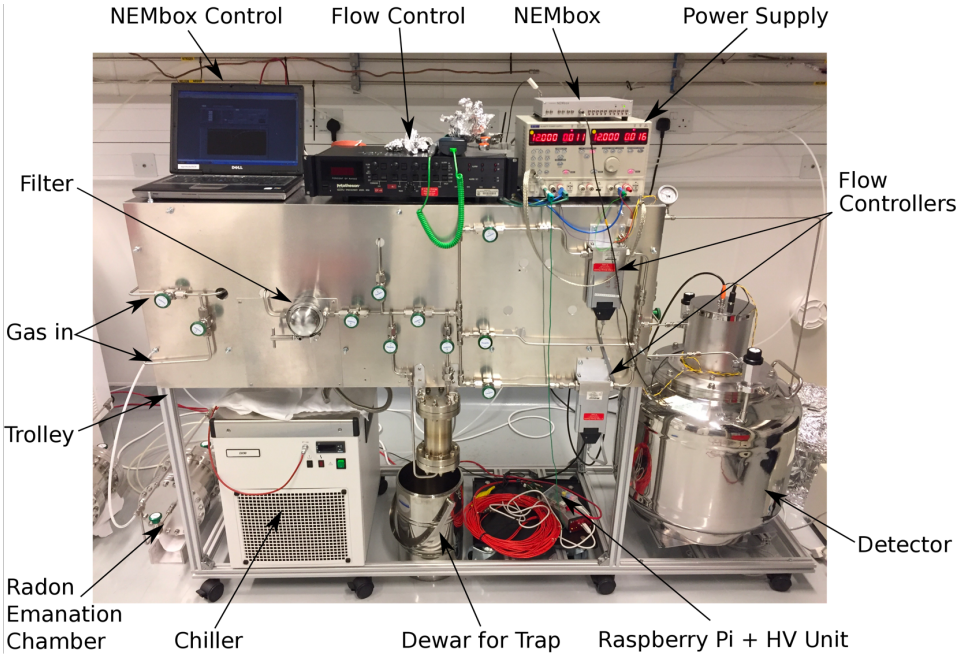

Figure 1.18: The set up of in Radon Concentration Line in real-life

1.4.2 Calibration

The trapping and transfer efficiency of RnCL must be determined so that the system can offer meaningful measurement results. There are mainly two methods to do this calibration.

The RnCL can be calibrated with the flowthrough method. The radon emanation of the SuperNEMO C-Sections are also measured using the RnCL via the flow-

through method, thus calibrating the RnCL under same conditions of the C-Section measurement can provide reliable results. The calibration procedure is described as follows.

1. First, flush the RnCL and detector with nitrogen to remove the residual radon and seal the detector afterwards. Attach the calibration radon source (same source as detector calibration) to the RnCL and then continuously flush nitrogen at 3 lpm through the source to the exhaust over at least 4 hours. This flushing procedure lasts for at least 4 hours, with the aim of clearing the residual radon and to wait for the residual polonium to decay away.

2. After 4 hours of zeroing the source, increase the flowrate to 7 lpm and divert the gas flow through the detector to the exhaust over 24 hours, to monitor the activity through the detector. The activity should remain stable after several hours' radon build-up until the end of the 24 hours' flushing. The flowrate of 7 lpm is selected in particular because it is the flowrate used in the real C section measurement, and it is also the highest achievable flowrate due to leaks on the C section at this stage.

3. After 24 hours flushing, start the trapping stage by diverting the gas to flow from the source through the cold trap (typically $<$ -50 °C in the central part of the trap) and detector to exhaust. The trap is cooled down via immersion in isopropanol inside a Dewar, and cooled by the refrigerator cooler (EK90 Immersion Cooler from Thermo Scientific).

4. After exactly 24 hours, seal the trap and source to stop trapping, and then remove the source. Also, stop cooling the trap and wait until the trap is warmed back to room temperature.

5. Start heating the trap to release radon and in the meantime flush the detector with 700 litres of helium to remove residual radon and replace the nitrogen environment inside the detector. As mentioned previously (see Section 1.1), the detector has a better detection efficiency working under a helium atmosphere.

6. When the trap is heated to over 200 °C, transfer the gas sample from the trap into the detector for measurement.

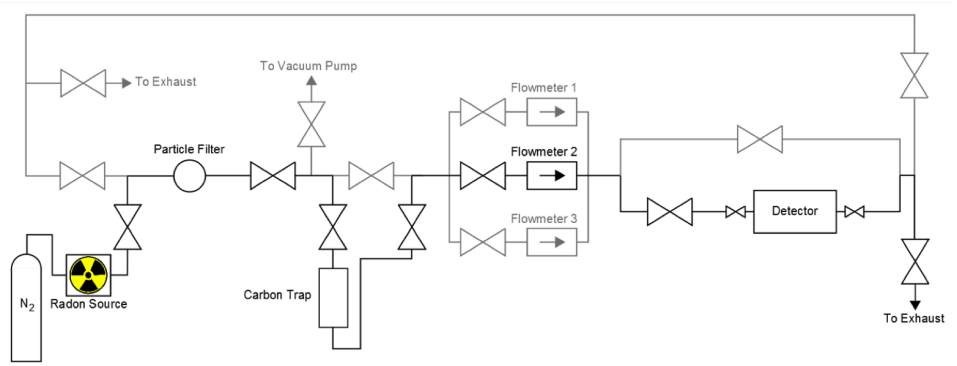

Figure 1.19: Schematic diagram of the setup during a flowthrough calibration of the RnCL.

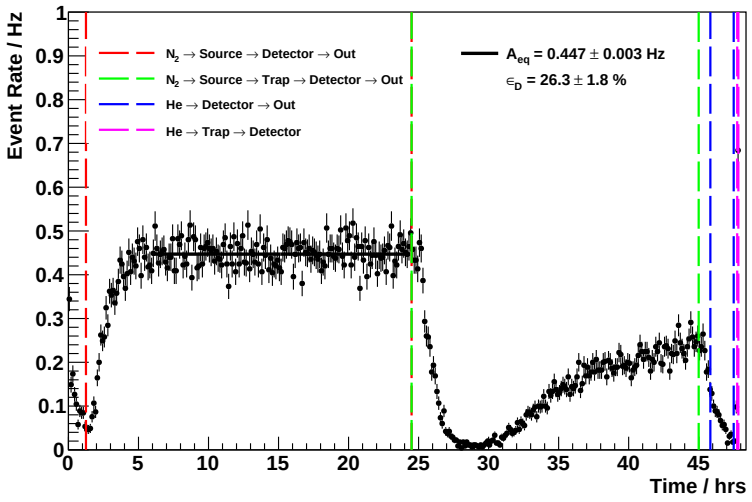

Figure 1.20: Typical ^{214}Po rates measured in the detector during the trapping stage of the RnCL flowthrough calibration measurement, with nitrogen as the carrier gas and a trap temperature of -50 °C.

The schematic diagram showing the trapping and transferring stage of the RnCL calibration using the flowthrough method is shown in Figure 1.19.

1.4.3 Sensitivity of RnCL

The MDA of the electrostatic detector was defined in Section 1.2.2. The RnCL is able to improve upon this MDA in terms of Bq/m^3 by allowing the measurement of the concentrated radon sample from a large volume of gas with the electrostatic

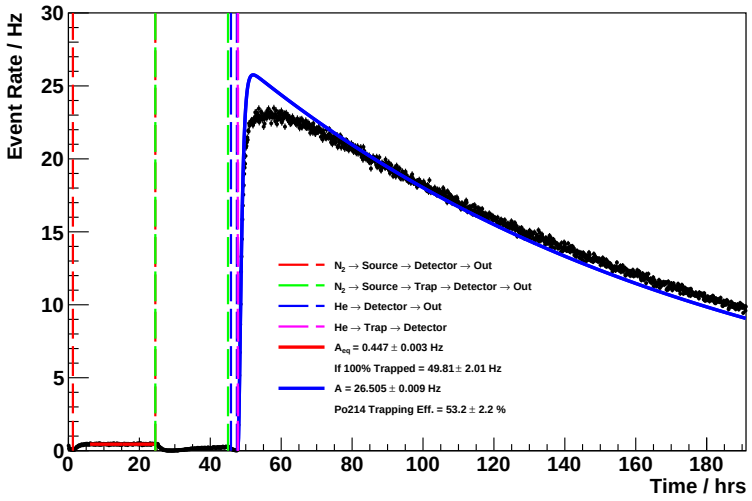

Figure 1.21: Typical ^{214}Po rates measured in the detector during the trapping and transfer stage of the RnCL flowthrough calibration measurement, with nitrogen flushing at 7 lpm.

detector. The MDA improves as a function of the volume of gas [5], as shown in Figure 1.23.

A significant improvement can be seen, and sensitivities as low as 5 μBq/m^3 can be achieved. The volume of gas required to improve the MDA increases exponentially. For a typical C-Section measurement, where 8.4 m^3 of gas is sampled, a sensitivity of < 20 μBq/m^3 can be reached, which is more than enough to meet the SuperNEMO radon target.

1.5 J-trap

The J-trap is a gas purification system developed and built at CPPM by J. Busto [10], which is designed to supply carrier gas with ultra-low and stable radon contamination by removing radon in the gas. Since all commercial gases contain relatively high and variable amounts of radon, the J-trap can remove the greatest sources of systematic uncertainties in measurement.

The J-trap is estimated to suppress the radon by a factor of 20 for nitrogen and 2×10^{10} for helium [10]. The trap consists of two freezers operating at -50 °C and -80

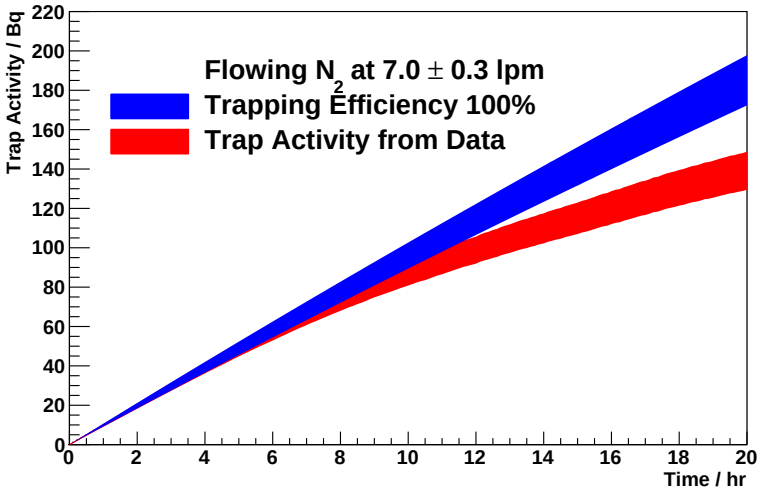

(a) Radon activity

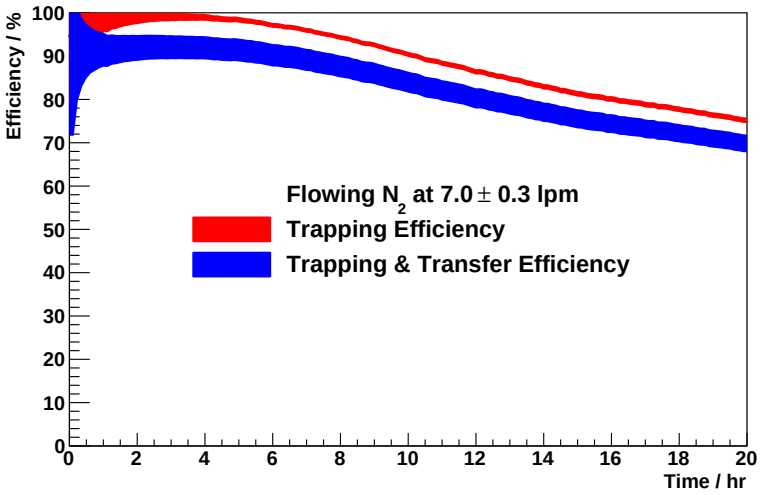

(b) Efficiency

Figure 1.22: (a) Radon activity inside the carbon trap during the flowthrough calibration of RnCL. The activity is calculated by measuring the trap output (red) and in the ideal trapping efficiency case (blue). (b) Ratio of the two lines in (a) giving the trapping efficiency (red) and the trapping and transfer efficiency (blue).

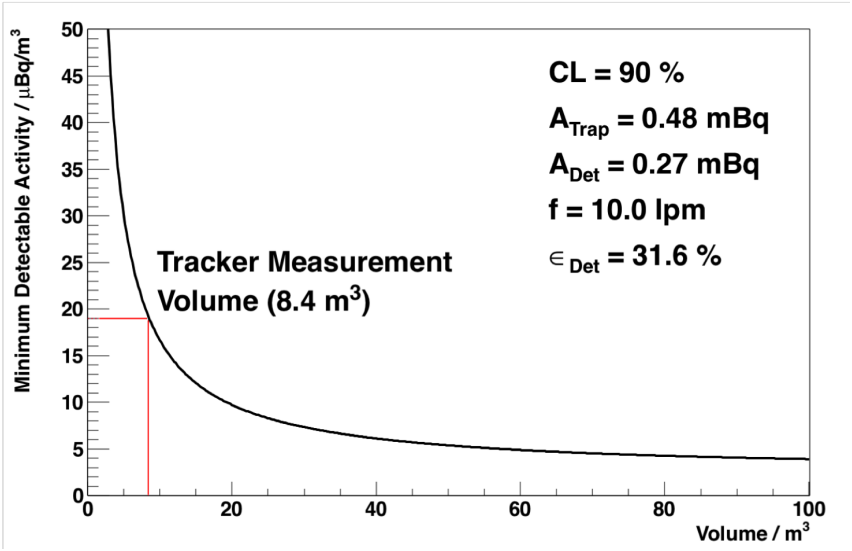

Figure 1.23: The Sensitivity (MDA) of RnCL for the C-Section measurement, as a function of the sample gas volume [6].

°C containing 3 and 1 stainless steel cartridge respectively, each housing 0.5 kg of active charcoal. The schematic of the J-trap is shown in Figure 1.24.

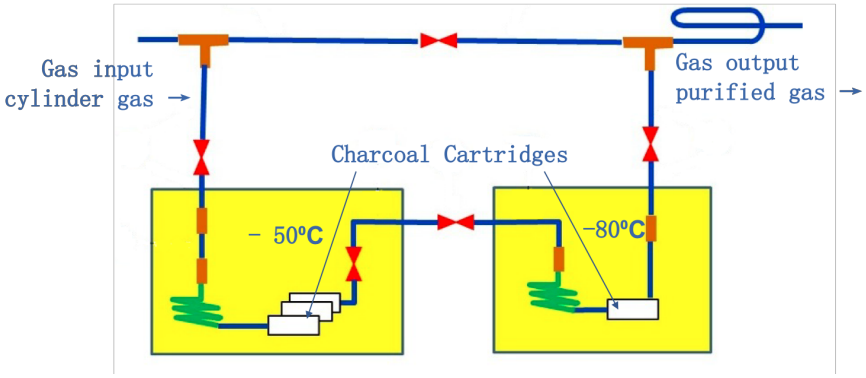

Figure 1.24: The schematic of the J-trap developed at CPPM [10].

When the carrier gas flow through the system, the active charcoal can adsorb radon. The low temperature improves the radon trapping efficiency of the charcoal as well

as suppressing the radon emanation of the charcoal itself. The system does not require very radio-pure charcoal to work, thus reducing the cost of building it. The charcoal cartridges can be replaced when needed, which provide more portability. The J-trap was delivered to MSSL and installed in May 2014, then moved to UCL and reassembled in October 2017. The temperature was monitored regularly to ensure it remained stable.

The principle of measuring the radon suppression of the J-trap is similar to a C-Section measurement [11], as described in Section **??**. The results of the radon contamination level of nitrogen after the J-trap are listed in Table 1.3 in comparison with cylinder nitrogen gas and cylinder helium.

Gas	Source	Radon Level (μBq/m^3)
He	Cylinder	70-100
N_2	Cylinder	400-1000
N_2	J-trap	20

Table 1.3: Measurements of cylinder helium and cylinder nitrogen and nitrogen from the J-trap [12].

There can be considerable variation of the radon activity among cylinders, and even within the same cylinder but different remaining activity [5]. With the J-trap, one of the most significant systematic uncertainties of the measurement involving a large volume of gas can be removed.

Bibliography

[1] E. Choi, M. Komori, K. Takahisa, N. Kudomi, K. Kume, K. Hayashi, S. Yoshida, H. Ohsumi, H. Ejiri, T. Kishimoto, K. Matsuoka, and S. Tasaka. Highly sensitive radon monitor and radon emanation rates for detector components. *Nucl.Instrum.Meth.*, A459:177–181, 2001.

[2] C. Mitsuda, T. Kajita, K. Miyano, S. Moriyama, and M. et al. Nakahata. Development of super-high sensitivity radon detector for the Super-Kamiokande detector. *Nucl.Instrum.Meth.*, A497:414–428, 2003.

[3] E.M. Wellisch. The distribution of the active deposit of radium in an electric field. *Philosophical Magazine Series 6*, 26(154):623–635, 1913.

[4] P. Pagelkopf and J. Porstendörfer. Neutralisation rate and the fraction of the positive ^{218}po-clusters in air. *Atmospheric Environment*, 37(8):1057 – 1064, 2003.

[5] J. E. Mott. *Search for double beta decay of ^{82}Se with the NEMO-3 detector and development of apparatus for low-level radon measurements for the SuperNEMO experiment*. PhD thesis, University College London, 2010.

[6] X. R. Liu. *Low background techniques for the SuperNEMO experiment*. PhD thesis, University College London, 2017.

[7] G.F. Knoll. Radiation Detection and Measurement. *ISBN-9780470131480*, 2000.

[8] X. R. Liu. Radio-purity Strategy for the SuperNEMO Experiment. *Internal Note*, DocDB:3986, 2016.

[9] G Heusser, W Rau, B Freudiger, M Laubenstein, M Balata, and T Kirsten. ^{222}rn detection at the range in nitrogen gas and a new rn purification technique for liquid nitrogen. *Applied Radiation and Isotopes*, 52(3):691 – 695, 2000.

[10] J. Busto. Design of a Preliminary Anti-Radon System. *Internal Note*, DocDB:3117, 2014.

[11] J. E. Mott. First radon measurements of C0, Internal SuperNEMO Technical Report. *Internal Note*, DocDB:2957, 2013.

[12] Xin Ran Liu. Ultra-low level radon assays in gases. *AIP Conference Proceedings*, 1672(1):070002, 2015.